

# Connecting multi-lepton anomalies at the LHC and in Astrophysics with MeerKAT/SKA

Geoff Beck<sup>1</sup> Ralekete Temo<sup>1</sup> Elias Malwa<sup>2</sup> Mukesh Kumar<sup>2</sup>  
Bruce Mellado<sup>2,3</sup>

<sup>1</sup>School of Physics and Centre for Astrophysics, University of the Witwatersrand, Johannesburg, Wits 2050, South Africa.

<sup>2</sup>School of Physics and Institute for Collider Particle Physics, University of the Witwatersrand, Johannesburg, Wits 2050, South Africa.

<sup>3</sup>iThemba LABS, National Research Foundation, PO Box 722, Somerset West 7129, South Africa.

E-mail: [geoffrey.beck@wits.ac.za](mailto:geoffrey.beck@wits.ac.za), [1497117@students.wits.ac.za](mailto:1497117@students.wits.ac.za), [elias.malwa@cern.ch](mailto:elias.malwa@cern.ch),  
[mukesh.kumar@cern.ch](mailto:mukesh.kumar@cern.ch), [bmellado@mail.cern.ch](mailto:bmellado@mail.cern.ch)

**Abstract.** Multi-lepton anomalies at the Large Hadron Collider (LHC) are reasonably well described by a two Higgs doublet model with an additional singlet scalar. Here, we demonstrate that using this model with parameters set by the LHC, we are also able to describe the excesses in gamma-ray flux from the galactic centre and the cosmic-ray spectra from AMS-02. This is achieved through Dark Matter (DM) annihilation via the singlet scalar. Of great interest is the flux of synchrotron emissions which results from annihilation of DM in Milky-Way satellites. We make predictions for MeerKAT/SKA observations of the nearby dwarf galaxy Reticulum II and we demonstrate the power of this instrument as a new frontier in indirect dark matter searches. Since the dark matter sector of the aforementioned two Higgs doublet model is unconstrained by current LHC data, we also demonstrate a synergy between particle and astrophysical searches in order to motivate further exploration of this promising model.

---

## Contents

<b>1</b>	<b>Introduction</b>	<b>1</b>
<b>2</b>	<b>MeerKAT telescope and the SKA</b>	<b>2</b>
<b>3</b>	<b>Particle physics model</b>	<b>3</b>
<b>4</b>	<b>Astrophysical modelling</b>	<b>3</b>
<b>5</b>	<b>Methodology</b>	<b>6</b>
<b>6</b>	<b>Results</b>	<b>8</b>
<b>7</b>	<b>Conclusions</b>	<b>13</b>

---

## 1 Introduction

The discovery of a Higgs boson ( $h$ ) [1–4] at the Large Hadron Collider (LHC) by the ATLAS [5] and CMS [6] experiments has opened a new chapter in particle physics. Measurements provided so far indicate that the quantum numbers of this boson are consistent with those predicted by the Standard Model (SM) [7, 8], and that the relative branching ratios (BRs) to SM particles are similarly well described. With this in mind, a window of opportunity now opens for the search for new bosons.

One of the implications of a two-Higgs doublet model with an additional singlet scalar  $S$  (2HDM+ $S$ ), is the production of multiple-leptons through the decay chain  $H \rightarrow Sh, SS$  [9], where  $H$  is the heavy CP-even scalar and  $h$  is considered as the SM Higgs boson with mass  $m_h = 125$  GeV. Excesses in multi-lepton final states were reported in Ref. [10]. In order to further explore results with more data and new final states, while avoiding biases and look-else-where effects, the parameters of the model were fixed in 2017 according to Refs. [9, 10]. This includes setting the scalar masses as  $m_H = 270$  GeV,  $m_S = 150$  GeV, treating  $S$  as a SM Higgs-like scalar and assuming the dominance of the decays  $H \rightarrow Sh, SS$ . Statistically compelling excesses in opposite sign di-leptons, same-sign di-leptons, and three leptons, with and without the presence of  $b$ -tagged hadronic jets were reported in Refs. [11–13]. Subsequently, with independent data sets and the phase-space fixed by the above mentioned model, an  $8\sigma$  combined excess was reported in [14], indicating a statistical preference for 2HDM+ $S$  over the SM alone. These excesses have continued to grow [12, 13, 15, 16]. With the procedure followed, the look-else-where or trials factors are nullified. In addition, a candidate of  $S$  with a mass of 151.5 GeV and a significance of  $4.8\sigma$  has just been reported in [15]. The possible connection with the anomalous magnetic moment of the muon  $g - 2$  was reported in Ref. [17]. For a review of various anomalies see [16].

Interestingly, the aforementioned 2HDM+ $S$  models can accommodate a DM candidate particle, whose production would contribute to “missing energy” in LHC measurements. As yet, the properties of this particle are not constrained by any of the data from the LHC used in [9–13]. This can be utilised to further test the 2HDM+ $S$  model in the context of astrophysical measurements, which indicate that baryonic matter comprises 5% of the current energy density in the universe while DM makes up more than 24% [18–22]. Thus, the DM candidate of the model could be expected to be probed by observations of regions with high DM density.

In this study we aim to use astrophysics as an indirect probe of the unconstrained elements of the 2HDM+ $S$  model that is, so far, motivated by LHC anomalies. This is done via a DM particle coupling to  $S$  as a mediator to the SM, where the non-DM parameters of the collider model are fixed to describe the LHC data [9, 23]. Since the DM candidate is unconstrained at the LHC, additional observational probes are needed to supplement the collider data. Thus, we will study the potential DM candidate parameter space while holding the other 2HDM+ $S$  parameters fixed.

We make particular use of the observed positron excess by the Alpha Magnetic Spectrometer (AMS-02) [24], anti-protons from the same detector [25], and the excess in gamma-ray fluxes from the galactic centre measured by Fermi-LAT [26]. This is partially motivated by the fact that the LHC anomalies triggering the 2HDM+S model are leptonic in nature. These particular astrophysical data sets are of interest as they have been extensively studied as potential signatures of DM [27–35]. This DM model is then used to make predictions for radio observations with the MeerKAT precursor to the Square Kilometre Array (SKA). These emissions would result from synchrotron radiation from electrons and positrons produced in DM annihilations. As such, we compute the number of  $e^+$  and  $p^-$  as a result of DM annihilations using the model described here from the collider physics perspective, and with the input from the astrophysics, we extend this by ensuring consistency with astrophysical observations. With a constrained DM model, our predictions can then be tested independently via observations with the MeerKAT telescope. In this regard, the complementarity between collider and astroparticle physics is investigated in the model considered here. Furthermore, the favoured DM candidate mass regions, resulting from astrophysical limits, can be used to motivate collider searches to better probe the properties of the 2HDM+S model.

This paper is structured as follows. Section 2 succinctly describes the MeerKAT telescope. The particle and astro-particle physics models are described in Sections 3 and 4, respectively. The methodology used here is detailed in Section 5. Results and conclusions are presented in Sections 6 and 7, respectively.

## 2 MeerKAT telescope and the SKA

Indirect detection of DM has been traditionally focused upon the use of gamma-ray experiments, such as the Fermi-LAT [36], because this mode of detection has low attenuation in the interstellar medium and has high detection efficiency. Recently, the indirect hunt for DM in radio-band has become prominent. This emerges from the fact that radio interferometers have an angular resolution vastly transcending that of gamma-ray experiments. Of particular interest to this work is the SKA, an international science project designed for studies in the field of radio astronomy. This telescope array provide around 50 times the sensitivity and 10,000 times the survey speed of the best current telescopes [37]. These capabilities have already been extensively argued to provide a powerful tool for exploring the properties of DM via indirect detection of annihilation or decay products [34, 35, 38]. At present, the precursor array MeerKAT is currently being operated by the South African Radio Astronomy Observatory (SARAO) with 64 antennae elements. Each of the elements is a 13.5 m diameter dish, configured to achieve high sensitivity and wide imaging of the sky. With 20 hours of time on target it is estimated that MeerKAT can achieve a point-source sensitivity of  $2.45 \mu\text{Jy beam}^{-1}$  at robust weighting 0, this is sourced from SARAO’s publicly available tools<sup>1</sup>. This results in an rms sensitivity of  $= 2.45 \mu\text{Jy beam}^{-1} \times \left(\frac{1 \text{ arcminute}}{11 \text{ arcseconds beam}^{-1}}\right)^2 \approx 73 \mu\text{Jy}$ , when taking into account the synthesized beam size of  $\approx 11$  arcseconds and assuming arcminute scale emissions. We note that a more tailored estimate of MeerKAT sensitivity, making use of an arcminute-scale taper on the visibilities, will likely yield an improved sensitivity. This is because the DM emission is diffuse and will be on a scale of arcminutes [39], while the visibility taper reduces contributions from long array baselines [40], corresponding to small angular scales, which would be dominated by the signal from point sources. Therefore,  $73 \mu\text{Jy}$  therefore constitutes a conservative estimate. Note that the impact of the taper would be somewhat reduced by the additional need for the subtraction of non-DM emission sources.

The sensitivity of MeerKAT is around a factor of 2 better than ATCA<sup>2</sup> which has previously been used for indirect DM searches in dwarf galaxies [39]. This notable sensitivity advantage is a consequence of the instrument exceeding its original design specifications, see [41] and [37], making it an unexpected new leader in radio-frequency DM searches. Additionally, MeerKAT is expected

<sup>1</sup>[https://archive-gw-1.kat.ac.za/public/tools/continuum\\_sensitivity\\_calculator.html](https://archive-gw-1.kat.ac.za/public/tools/continuum_sensitivity_calculator.html)

<sup>2</sup>[https://www.narrabri.atnf.csiro.au/myatca/interactive\\_senscalc.html](https://www.narrabri.atnf.csiro.au/myatca/interactive_senscalc.html)

to receive an upgrade of an additional 20 dishes, taking it to 84, with construction expected to be complete in 2023.<sup>3</sup>

When computing SKA sensitivities we make use of Tables 6 and 7 from [42] we perform a similar scaling to get  $\mu\text{Jy arcmin}^{-2}$  as with MeerKAT, but we use the geometric mean of quoted minimum and maximum beam sizes. This will likely result in conservative estimates for the sensitivity.

### 3 Particle physics model

Here, we succinctly describe the model used to describe the multi-lepton anomalies observed in the LHC data and with which to interpret the above mentioned excesses in astrophysics. The formalism is comprised of a model of fundamental interactions interfaced with a model of cosmic-ray fluxes that emerge from DM annihilation. The potential for a two Higgs-doublet model with an additional real singlet field  $\Phi_S$  (2HDM+S) is given as in Ref. [9]:

$$\begin{aligned}
V(\Phi) = & m_{11}^2 |\Phi_1|^2 + m_{22}^2 |\Phi_2|^2 - m_{12}^2 (\Phi_1^\dagger \Phi_2 + \text{h.c.}) + \frac{\lambda_1}{2} (\Phi_1^\dagger \Phi_1)^2 + \frac{\lambda_2}{2} (\Phi_2^\dagger \Phi_2)^2 \\
& + \lambda_3 (\Phi_1^\dagger \Phi_1) (\Phi_2^\dagger \Phi_2) + \lambda_4 (\Phi_1^\dagger \Phi_2) (\Phi_2^\dagger \Phi_1) + \frac{\lambda_5}{2} [(\Phi_1^\dagger \Phi_2)^2 + \text{h.c.}] \\
& + \frac{1}{2} m_S^2 \Phi_S^2 + \frac{\lambda_6}{8} \Phi_S^4 + \frac{\lambda_7}{2} (\Phi_1^\dagger \Phi_1) \Phi_S^2 + \frac{\lambda_8}{2} (\Phi_2^\dagger \Phi_2) \Phi_S^2.
\end{aligned} \tag{3.1}$$

The fields  $\Phi_1, \Phi_2$  in the potential are the  $SU(2)_L$  Higgs doublets. The first three lines in Eq. (3.1) are the contributions of the real 2HDM potential. The terms of the last line are contributions of the singlet field  $\Phi_S$ . To prevent the tree-level flavour changing neutral currents we consider a  $\mathbb{Z}_2$  symmetry which can be softly broken by the term  $m_{12}^2 \neq 0$ . After the minimisation of the potential and electro-weak symmetry breaking, the scalar sector is populated with three  $CP$  even scalars  $h$  (SM Higgs),  $H$  and  $S$ , one  $CP$  odd scalar  $A$  and charged scalar  $H^\pm$ . For more details of this model and associated interactions' Lagrangians and parameter space we refer to Refs. [9, 23]. Further, we consider interactions of  $S$  with three types of DM candidates  $\chi_r, \chi_d$  and  $\chi_v$  with spins 0, 1/2 and 1, respectively:

$$\mathcal{L}_{int} = \frac{1}{2} M_{\chi_r} g_{\chi_r}^S \chi_r \chi_r S + \bar{\chi}_d (g_{\chi_d}^S + i g_{\chi_d}^P \gamma_5) \chi_d S + g_{\chi_v}^S \chi_v^\mu \chi_{v\mu} S, \tag{3.2}$$

where  $g_{\chi_i}$  and  $M_{\chi_i}$  are the coupling strengths of DMs with the singlet real scalar  $S$  and masses of DM, respectively. Having these interactions in mind, we consider DM annihilation through  $S$  following  $2 \rightarrow 2$  and  $2 \rightarrow 3$  scattering. These respectively correspond to the processes  $\chi \bar{\chi} \rightarrow S \rightarrow X$  and  $\chi \bar{\chi} \rightarrow S \rightarrow H S/h \rightarrow X$  (where  $X$  represents some Standard Model products). It is important to note that the non-DM model parameters for the 2HDM+S model are fixed according to [9, 10]. Since the  $S$  boson is assumed to have Higgs-like branching ratios to the SM, the mass of these particles will directly effect the  $\chi\chi$  SM products as the ratios scale with Higgs mass. Additionally, for simplicity we have only considered interactions where the 2HDM+S particles are not produced virtually, thus limiting the minimum DM mass considered.

Additionally, the DM candidate degree of freedom is, as yet, unconstrained by LHC data. Therefore, we will scan a wide parameter space, from the lowest DM masses that can produce  $S$  bosons up to 1 TeV. In the  $2 \rightarrow 3$  case the lower mass limit is that required to produce  $H$  and  $h$  bosons together. In this regard, astrophysical searches will compliment LHC data by probing aspects of the 2HDM+S model that is unconstrained by collider data.

### 4 Astrophysical modelling

In terms of modelling fluxes of cosmic-rays at Earth due to DM annihilation, we use the propagation functions from Ref. [43] and consider all three diffusion scenarios (the extremal MIN and

<sup>3</sup><https://www.mpg.de/15382572/top-radio-telescope-in-south-africa>

MAX, as well as the more moderate MED case). For predicting multi-frequency photon fluxes we follow Ref. [34] in using a Green's function method of solving for equilibrium electron distributions in the halo environment, under the assumption that diffusion and loss functions do not vary spatially. We will consider synchrotron, gamma-ray, inverse-Compton, and bremsstrahlung radiation from annihilation products using the emission power equations from [35].

The principle equation of interest in this work will be the diffusion-loss equation for a particle species  $i$ :

$$\frac{\partial}{\partial t} \frac{dn_i}{dE} = \vec{\nabla} \cdot \left( D(E, \vec{x}) \vec{\nabla} \frac{dn_i}{dE} \right) + \frac{\partial}{\partial E} \left[ b(E, \vec{x}) \frac{dn_i}{dE} \right] + Q_i(E, \vec{x}), \quad (4.1)$$

where  $D$  is the diffusion function,  $b$  is the energy-loss function,  $Q_i$  is the source function for  $i$ -particles, and  $\frac{dn_i}{dE} = \frac{dn_i}{dE}(E, \vec{x})$  is the number density per unit energy of  $i$ -particles. In particular, the equilibrium solutions of Eq. (4.1) will provide the distributions of particles injected by DM annihilations within a given astrophysical environment.

In the case of positrons, the source function  $Q_{e^+}$  is then given by:

$$Q_{e^+} = \frac{1}{2} \left( \frac{\rho_\chi(\vec{x})}{M_\chi} \right)^2 \langle \sigma V \rangle \frac{dn_{e^+}}{dE} \Big|_{\text{inj}}, \quad (4.2)$$

where  $\frac{dn_{e^+}}{dE} \Big|_{\text{inj}}$  is the injected number density of positrons per unit energy,  $\rho_\chi(\vec{x})$  is the DM density at  $\vec{x}$ , and  $\langle \sigma V \rangle$  is the velocity averaged annihilation cross-section for DM particles. The function  $D(E, \vec{x})$  depends upon assumptions about the Milky-Way diffusion environment [44] and we explore all three value sets MIN, MED, and MAX presented in Ref. [43]. The equilibrium solution  $\frac{dn_{e^+}}{dE}$  to Eq. (4.1) taken from Ref. [43] can then be leveraged to obtain the flux in the solar neighbourhood via:

$$\frac{d\Phi_{e^+}}{dE} = \frac{c \langle \sigma V \rangle}{8\pi b(E)} \left( \frac{\rho_\odot}{M_\chi} \right)^2 \int_E^{M_\chi} dE_s \frac{dn_{e^+}}{dE_s} \Big|_{\text{inj}} I_\odot(E, E_s), \quad (4.3)$$

where  $E_s$  is the energy of injected positrons, and  $I_\odot(E, E_s)$  is a Green's function solving Eq. (4.1) at the location of Earth, this being given by Ref. [43].

Similarly, the anti-proton flux in the solar neighbourhood can be determined, according to Ref. [43], as being given by:

$$\frac{d\Phi_{\bar{p}}}{dK} = \frac{v_{\bar{p}}}{8\pi} \langle \sigma V \rangle \left( \frac{\rho_\odot}{M_\chi} \right)^2 R(K) \langle \sigma V \rangle \frac{dn_{\bar{p}}}{dK} \Big|_{\text{inj}}, \quad (4.4)$$

where  $K$  is anti-proton kinetic energy,  $v_{\bar{p}}$  is the anti-proton speed,  $R(K)$  are the propagation functions from Ref. [43], and  $\frac{dn_{\bar{p}}}{dK} \Big|_{\text{inj}}$  is the injected anti-proton spectrum.

Primary photon fluxes within radius  $r$  of a halo centre, at frequency  $\nu$  are found via:

$$S_\gamma(\nu, r) = \int_0^r d^3r' \frac{Q_\gamma(\nu, r')}{4\pi(d_L^2 + (r')^2)}, \quad (4.5)$$

where  $Q_\gamma$  is the photon source function of similar form to Eq. (4.2), and where  $d_L$  is the luminosity distance to the halo centre. The integral in Eq. (4.5) will taken over some chosen region of interest in each studied target.

Secondary photon fluxes (from electrons produced by DM annihilation) are found using the equations:

$$j_i(\nu, r) = \int_0^{M_\chi} dE \frac{dn_{e^\pm}}{dE}(E, r) P_i(\nu, E, r), \quad (4.6)$$

where  $\frac{dn_{e^\pm}}{dE}$  is the sum of the electron and positron distributions (equilibrium solutions to Eq. (4.1)) within the source region and  $P_i$  is the power emitted at frequency  $\nu$  through mechanism  $i$  by an

electron with energy  $E$ , at position  $r$ . The flux produced within a radius  $r$  is then found via:

$$S_i(\nu, r) = \int_0^r d^3 r' \frac{j_i(\nu, r')}{4\pi(d_L^2 + (r')^2)}. \quad (4.7)$$

As the environment we consider is one of a dwarf galaxy we must take diffusion into account [45]. Thus, for all secondary fluxes we solve Eq. (4.1 with a Green's function method. Assuming spherical symmetry, we have that [45–48]:

$$\frac{dn_e}{dE}(r, E) = \frac{1}{b(E)} \int_E^{M_\chi} dE' G(r, E, E') Q_e(r, E'), \quad (4.8)$$

this solution method requires that  $b$  and  $D$  have no spatial dependency, thus they are defined

$$D(E) = D_0 \left( \frac{d_0}{1 \text{ kpc}} \right)^{\frac{2}{3}} \left( \frac{\bar{B}}{1 \mu\text{G}} \right)^{-\frac{1}{3}} \left( \frac{E}{1 \text{ GeV}} \right)^{\frac{1}{3}}, \quad (4.9)$$

where  $D_0 = 3.1 \times 10^{28} \text{ cm}^2 \text{ s}^{-1}$  [49],  $d_0$  is the magnetic field coherence length,  $\bar{B}$  is the average magnetic field strength, and  $E$  is the electron energy. The loss-function is found via [47, 50]:

$$\begin{aligned} b(E) = & b_{\text{IC}} \left( \frac{E}{1 \text{ GeV}} \right)^2 + b_{\text{sync}} \left( \frac{E}{1 \text{ GeV}} \right)^2 \left( \frac{\bar{B}}{1 \mu\text{G}} \right)^2 \\ & + b_{\text{Coul}} \left( \frac{\bar{n}}{1 \text{ cm}^{-3}} \right) \left( 1 + \frac{1}{75} \log \left( \frac{\gamma}{\left( \frac{\bar{n}}{1 \text{ cm}^{-3}} \right)} \right) \right) + b_{\text{brem}} \left( \frac{\bar{n}}{1 \text{ cm}^{-3}} \right) \left( \frac{E}{1 \text{ GeV}} \right), \end{aligned} \quad (4.10)$$

where  $\bar{n}$  is the average gas density, the coefficients  $b_{\text{IC}}$ ,  $b_{\text{sync}}$ ,  $b_{\text{Coul}}$ ,  $b_{\text{brem}}$  are the energy-loss rates from ICS, synchrotron emission, Coulomb scattering, and bremsstrahlung. These coefficients are given by  $0.25 \times 10^{-16} (1+z)^4$  (for CMB target photons),  $0.0254 \times 10^{-16}$ ,  $6.13 \times 10^{-16}$ ,  $4.7 \times 10^{-16}$  in units of  $\text{GeV s}^{-1}$ . The average quantities  $\bar{n}$  and  $\bar{B}$  are computed by weighting the average with  $\rho_\chi^2$ , ensuring they accurately reflect the environment of the majority of annihilations.

The Green's function is then given by:

$$\begin{aligned} G(r, E, E') = & \frac{1}{\sqrt{4\pi\Delta v}} \sum_{n=-\infty}^{\infty} (-1)^n \int_0^{r_{\text{max}}} dr' \frac{r'}{r_n} \\ & \times \left( \exp \left( -\frac{(r' - r_n)^2}{4\Delta v} \right) - \exp \left( -\frac{(r' + r_n)^2}{4\Delta v} \right) \right) \frac{Q_e(r')}{Q_e(r)}, \end{aligned} \quad (4.11)$$

with the sum running over a set of image charges, each at position  $r_n = (-1)^n r + 2nr_{\text{max}}$ , where  $r_{\text{max}} = 2r_{\text{vir}}$  or twice the virial radius. The additional required definitions have:

$$\Delta v = v(u(E)) - v(u(E')), \quad (4.12)$$

with

$$\begin{aligned} v(u(E)) &= \int_{u_{\text{min}}}^{u(E)} dx D(x), \\ u(E) &= \int_E^{E_{\text{max}}} \frac{dx}{b(x)}, \end{aligned} \quad (4.13)$$

where  $E_{\text{max}} = m_\chi$ .

For synchrotron emission we then have [51, 52]:

$$P_{\text{sync}}(\nu, E, r) = \int_0^\pi d\theta \frac{\sin^2 \theta}{2} 2\pi \sqrt{3} r_e m_e c \nu_g F_{\text{sync}} \left( \frac{\kappa}{\sin \theta} \right), \quad (4.14)$$

where  $\nu_g$  is the non-relativistic gyro-frequency,  $r_e$  is the electron radius,  $m_e$  is the electron mass, and  $\theta$  is the angle between the magnetic field and electron trajectory. The value of  $\kappa$  is found via:

$$\kappa = \frac{2\nu}{3\nu_g\gamma^2} \left[ 1 + \left( \frac{\gamma\nu_p}{\nu} \right)^2 \right]^{\frac{3}{2}}, \quad (4.15)$$

with  $\gamma = \frac{E}{m_e c^2}$ . Finally,

$$F_{\text{sync}}(x) \simeq 1.25x^{\frac{1}{3}}e^{-x} (648 + x^2)^{\frac{1}{2}}. \quad (4.16)$$

The power produced by the inverse-Compton scattering (ICS) at a photon of frequency  $\nu$  from an electron with energy  $E$  is given by Ref. [51, 52]:

$$P_{\text{IC}}(\nu, E) = cE_\gamma(z) \int d\epsilon n(\epsilon)\sigma(E, \epsilon, E_\gamma), \quad (4.17)$$

where  $\epsilon$  is the energy of the seed photons distributed according to  $n(\epsilon)$  (this will taken to be that of the CMB), and

$$\sigma(E, \epsilon, E_\gamma) = \frac{3\sigma_T}{4\epsilon\gamma^2} G(q, \Gamma_e), \quad (4.18)$$

with  $\sigma_T$  being the Thompson cross-section and

$$G(q, \Gamma_e) = 2q \ln q + (1 + 2q)(1 - q) + \frac{(\Gamma_e q)^2(1 - q)}{2(1 + \Gamma_e q)}, \quad (4.19)$$

with

$$q = \frac{E_\gamma}{\Gamma_e(\gamma m_e c^2 + E_\gamma)}, \quad \Gamma_e = \frac{4\epsilon\gamma}{m_e c^2}, \quad (4.20)$$

where  $m_e$  is the electron mass.

Finally, the power from bremsstrahlung at photon energy  $E_\gamma$  from an electron at energy  $E$  is given by [51, 52]:

$$P_{\text{brem}}(E_\gamma, E, r) = cE_\gamma \sum_j n_j(r)\sigma_B(E_\gamma, E), \quad (4.21)$$

where  $n_j$  is the distribution of target nuclei of species  $j$  and the cross-section is given by:

$$\sigma_B(E_\gamma, E) = \frac{3\alpha\sigma_T}{8\pi E_\gamma} \left[ \left( 1 + \left( 1 - \frac{E_\gamma}{E} \right)^2 \right) \phi_1 - \frac{2}{3} \left( 1 - \frac{E_\gamma}{E} \right) \phi_2 \right], \quad (4.22)$$

with  $\phi_1$  and  $\phi_2$  being energy dependent factors determined by the species  $j$  (see [51, 52]).

## 5 Methodology

We use a Monte Carlo (MC) generator to simulate the production of particles as a result of the annihilation of DM through  $S$  according to the model described in Section 3. We make use of `MG5_@MC` [53] as our primary tool to generate events for the  $2 \rightarrow 2$  and  $2 \rightarrow 3$  scattering processes. The MC generator is interfaced with `Pythia 8` [54] to hadronize intermediate partons. We varied the DM mass between 200 to 1000 GeV for the  $2 \rightarrow 3$  scattering and 75 to 1000 GeV for the  $2 \rightarrow 2$  scattering with 100 GeV spacing. In Fig. 1 we display a complete set of yield spectra for positrons and anti-protons for  $2 \rightarrow 2$  and  $2 \rightarrow 3$  scattering. These graphs display the number of particles per annihilation per unit energy,  $dN/dE$ , and the yield functions binned in energy intervals of 0.5 GeV. Results are displayed for spin-0 DM. The resulting particle distributions are then used as inputs for indirect DM detection following Eqs. (4.3) and (4.4) in the case of the anti-proton and positron fluxes at Earth, and Eq. (4.7) for multi-frequency photon spectra. The subsequent analysis has two components. The first is constraining the allowed DM parameter space (in terms of  $M_\chi$  and  $\langle\sigma V\rangle$ ) using cosmic-ray and gamma-ray data. After this step we make predictions for MeerKAT

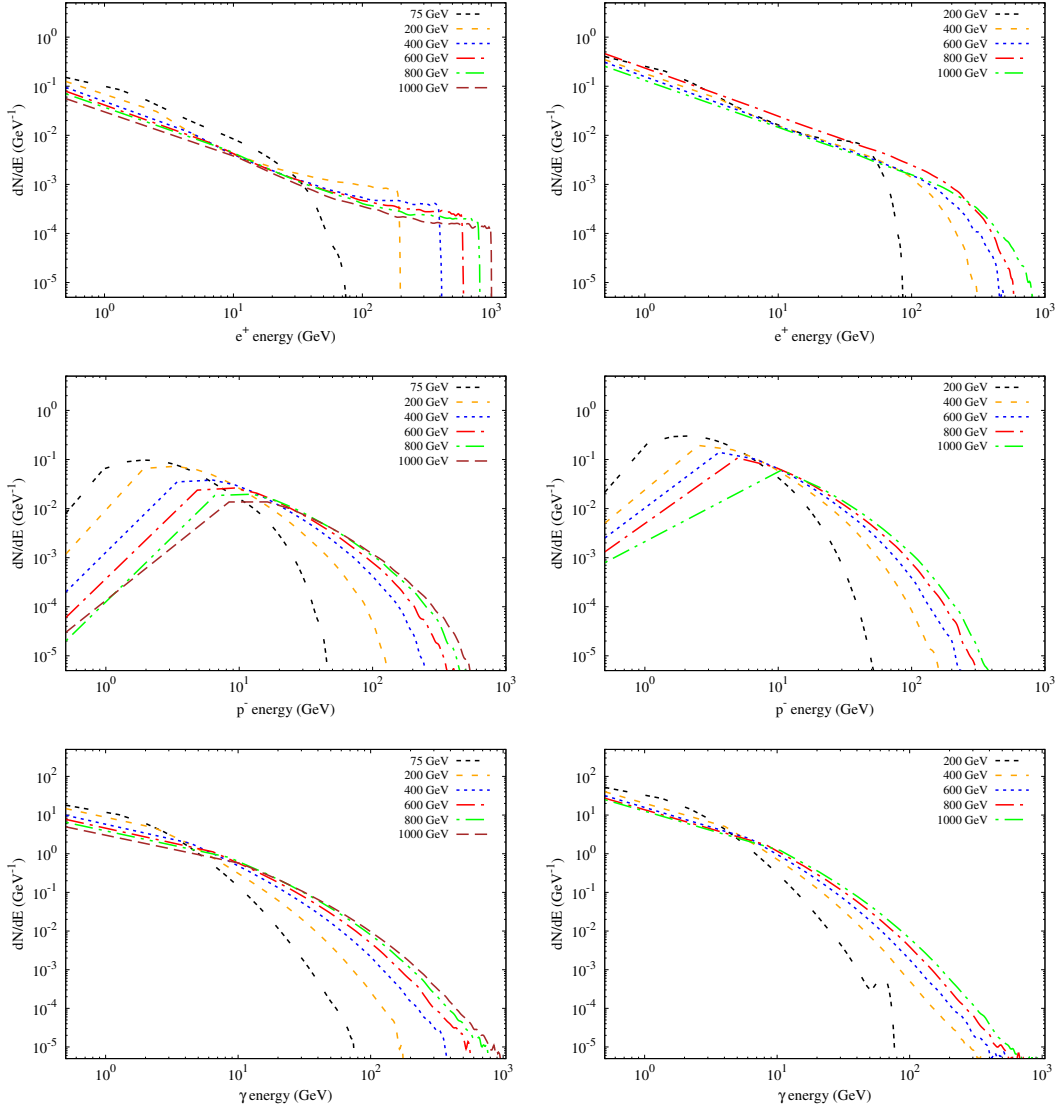


**Figure 1.** Differential yields of positrons, anti-protons and photons for the 2→2 (Left graphs) and 2→3 (Right graphs) annihilation scattering of Spin-0 DM masses. Model parameters are fixed according to Refs. [9, 10], based on LHC data.

observations based upon the constrained DM parameter space. The predicted spectra for cosmic-ray fluxes at Earth are compared to data from AMS-02 [24, 25]. In the case of the anti-protons we use the background model found in [55], while for positrons we use a nearby pulsar model for the high-energy background [56] (note that this means the DM component is sub-dominant). When we model gamma-ray fluxes from the galactic centre we use fiducial model data from Ref. [26], making use of the excess spectrum for a  $10^\circ$  region of interest around the galactic centre. In all cases our Milky-Way halo models follow those presented in Ref. [43].

We note that both AMS-02 anomalies have been widely studied, either as constraints on DM models or as potential signatures thereof [27–33]. The anti-proton case has been argued to be highly significant and most in agreement with the annihilation via  $b$ -quarks of a 40 – 70 GeV WIMP with some potential for heavier masses [27]. However, an accounting for possibility of correlated errors [55] reveals no preference for a DM contribution from WIMPS between 10 and



1000 GeV in mass. It is also difficult to reconcile such models with existing radio data [34]. In the case of positrons there is a stark but unexplained excess of positrons at around a few hundred GeV that can potentially be described in terms of DM models and has great potential to be used as a probe of DM physics even with astrophysical backgrounds [57]. Additionally, we note that the significance of the widely studied Fermi-LAT galactic centre gamma-ray excess is highly uncertain due to systematics [26]. Notably, [58] has recently argued that the galactic centre excess remains compatible with a contracted NFW [59] profile (see also the review in [16]).

## 6 Results

In Fig. 2 we display the best-fit parameter space for  $2 \rightarrow 2$  scattering with the AMS-02 positron data from [24] and the over-lap regions with the anti-proton and Fermi-LAT galactic centre gamma-ray parameter spaces. In order to account for uncertainties in the modelling of Milky-way DM halo we display the thermal relic cross-section [60] as a band, in order to represent the fact that models within this band are compatible with the relic value up to systematic uncertainties. The uncertainties are derived entirely from estimates of  $\rho_\odot$  (see for instance [61] and [62]). The plots in Fig. 2 show that crucial overlap regions fall slightly above the relic band. The regions for all three excesses do not mutually overlap, although it must be noted that systematic issues with the positron and gamma-ray data [24, 26] indicate that there may be missing ingredients in the astrophysical modelling. Despite this, the 3 regions cluster close together and converge close to the relic region. The presented figure shows the best-case overlap which requires the MED diffusion scenario and an Einasto (or NFW) halo with the parameters drawn from Ref. [43]. The fact that the uncontracted Einasto and NFW halos produced a closer agreement means that this overlap does not favour a more speculative contracted halo (as is often necessary for DM modelling of these excesses historically) and is compatible with non-extremal diffusion conditions. This stands in contrast with model independent searches like [58], where it is argued that a contracted DM profile is favoured for a DM-related explanation of the galactic centre excess spectrum from [26]. It is notable that despite our inclusion of a large positron background from a nearby pulsar [56] the favoured cross-sections remain large, indicating that DM is still playing a role in reconciling the AMS-02 positron data. We have made some initial verification that the parameter space of the 2HDM+ $S$  model that describes LHC and astro-physics data are not excluded by direct DM searches. In particular, for a Type-II 2HDM+ $S$  limits become weak when the ratio of the vacuum expectation values of the complex doublets,  $\tan\beta < 1$  [63], which is preferred by the LHC data [23]. This evasion of direct detection is possible as  $S$  acts as a mediator between DM and the SM and is not produced directly from the SM at the LHC (it results from  $H$  decays). This allows the direct signal to remain small without affecting the collider or indirect results. However, more in-depth analysis may be needed on this point. The best-fit DM parameter spaces are summarised in Tables 1 and 2.

Here, we display a comparison between the sensitivity of the MeerKAT telescope and the predicted emissions for our constrained DM model using the Reticulum II dwarf galaxy. The choice of this target is motivated by the fact that it is in an ideal location for southern hemisphere observations and has one of the highest ‘J-factors’ among known dwarf galaxies [64]. In fitting with our AMS-02 constraints from Fig. 2, we assume  $\langle\sigma V\rangle = 10^{-25} \text{ cm}^3 \text{ s}^{-1}$  and include uncertainties on the value of  $\rho_\odot$ . We make use of a cored density profile following arguments from Ref. [65, 66]. This being an Einasto profile [67] (which can be cored for certain parameter choices), given by:

$$\rho_e(r) = \rho_s \exp\left[-\frac{2}{\alpha}\left(\left[\frac{r}{r_s}\right]^\alpha - 1\right)\right], \quad (6.1)$$

where we follow Ref. [39] in having  $\alpha = 0.4$ ,  $r_s = 0.2 \text{ kpc}$ , and  $\rho_s = 7 \times 10^7 \text{ M}_\odot \text{ kpc}^{-3}$ . We then follow Ref. [39] in using the profiles for gas density and magnetic field strength:

$$n_e(r) = n_0 \exp\left(-\frac{r}{r_d}\right), \quad B(r) = B_0 \exp\left(-\frac{r}{r_d}\right). \quad (6.2)$$

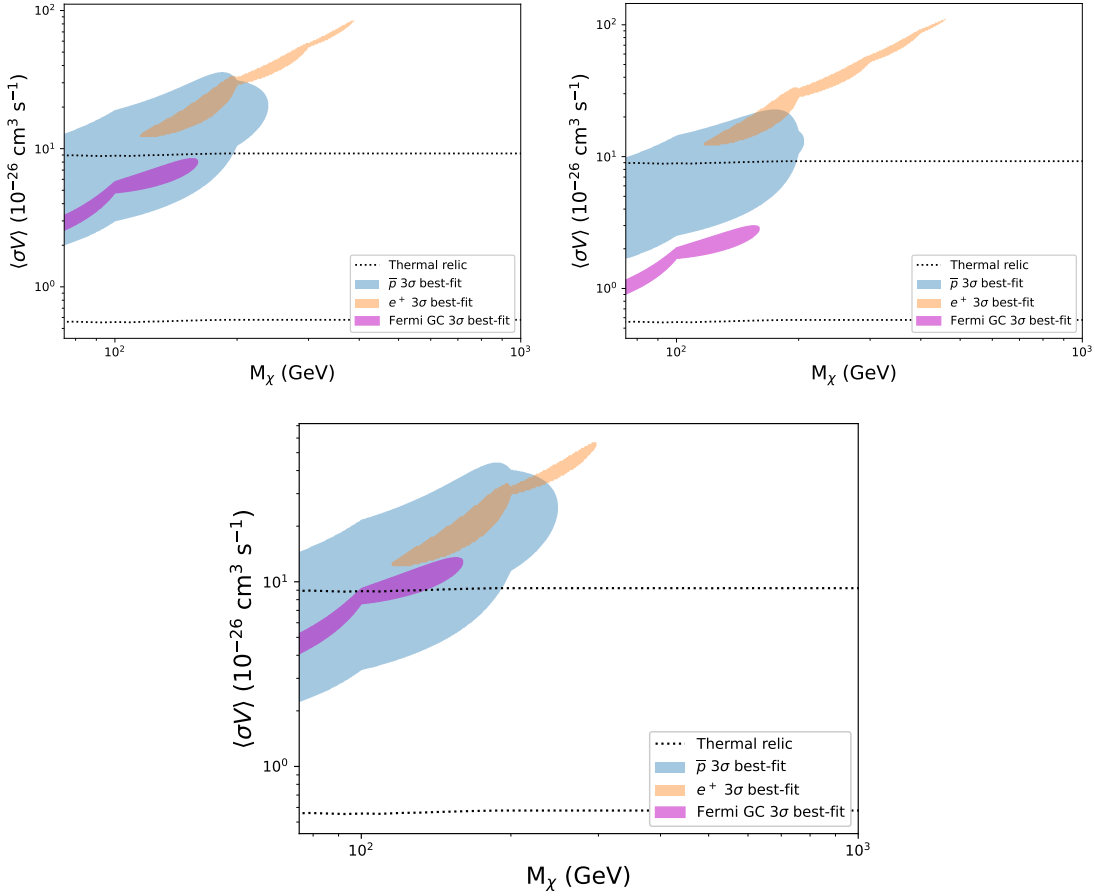


**Figure 2.** The parameter space fitting the  $2 \rightarrow 2$  scattering to the Fermi-LAT galactic centre excess, AMS-02 anti-proton and positron spectra. The shaded regions represent the  $3\sigma$  confidence interval. The region between the thermal relic lines represents the uncertainties in local DM density and galactic halo profile. This plot assumes the MED diffusion scenario. Top left: Einasto profile for the Milky-Way halo from Ref. [43]. Top right: contracted Einasto profile for the Milky-Way halo from Ref. [43]. Bottom: NFW profile for the Milky-Way halo from Ref. [43].

**Figure 3.** The parameter space fitting the  $2 \rightarrow 2$  scattering to the Fermi-LAT galactic centre excess, AMS-02 anti-proton and positron spectra. The shaded regions represent the  $3\sigma$  confidence interval. The region between the thermal relic lines represents the uncertainties in local DM density and galactic halo profile. This plot assumes the MED diffusion scenario and a

We take  $r_d$  to be given by the stellar-half-light radius with a value of 35 pc [68, 69] and we assume  $B_0 \approx 1 \mu\text{G}$ ,  $n_0 \approx 10^{-6} \text{ cm}^{-3}$ . The region of flux integration are taken as 3 arcminutes for radio and 30 arcminutes for gamma-rays. The first is in keeping with our assumption of arcminute scale emissions when determining sensitivity. The second is to reflect Fermi-LAT observations from [64].

Fig. 4 shows that Reticulum II with the Einasto profile produces radio fluxes detectable at  $2\sigma$  confidence interval with MeerKAT across the mass range (although the  $2 \rightarrow 2$  200 GeV case is very marginal). Only the lower masses are detectable at  $5\sigma$ . However, the entire uncertainty band is not covered in either case. It should be noted that the  $2 \rightarrow 3$  case presents slightly stronger emissions. Importantly, we also display the estimated sensitivity of the full SKA [42] which manages to probe the entire uncertainty region for both  $2 \rightarrow 2$  and  $2 \rightarrow 3$  processes at  $5\sigma$  confidence interval within 100 hours of observing time.

$M_\chi$ (GeV)	Lower ( $10^{-26} \text{ cm}^3 \text{ s}^{-1}$ )	Upper ( $10^{-26} \text{ cm}^3 \text{ s}^{-1}$ )	$M_\chi$ (GeV)	Lower ( $10^{-26} \text{ cm}^3 \text{ s}^{-1}$ )	Upper ( $10^{-26} \text{ cm}^3 \text{ s}^{-1}$ )
75.0	2.6	3.3	115.2	12.1	12.4
81.1	2.9	3.7	134.7	12.7	16.6
87.1	3.3	4.2	154.2	14.4	21.3
93.2	3.8	4.8	173.7	17.1	27.2
99.2	4.7	5.7	193.2	23.5	33.5
105.3	4.9	6.1	212.8	30.0	35.3
111.3	5.0	6.4	232.3	32.7	40.2
117.4	5.1	6.7	251.8	36.3	44.7
123.5	5.3	7.1	271.3	41.2	50.7
129.5	5.5	7.4	290.9	48.2	56.7
135.6	5.7	7.7	310.4	56.2	61.0
141.6	6.1	8.0	329.9	61.0	66.9
147.7	6.4	8.3	349.4	66.5	72.9
153.8	6.9	8.4	369.0	73.4	79.3
159.8	7.8	8.2	388.5	84.3	86.3

$M_\chi$ (GeV)	Lower ( $10^{-26} \text{ cm}^3 \text{ s}^{-1}$ )	Upper ( $10^{-26} \text{ cm}^3 \text{ s}^{-1}$ )
75.0	2.0	12.8
86.7	2.4	15.3
98.4	2.9	18.5
110.1	3.2	20.7
121.8	3.5	22.8
133.5	3.8	25.2
145.2	4.2	28.0
156.9	4.8	31.0
168.6	5.5	33.8
180.3	6.6	35.7
192.0	8.4	34.9
203.7	10.9	30.9
215.4	12.2	29.5
227.1	14.3	27.2
238.8	19.7	21.2

**Table 1.** The  $3\sigma$  confidence interval best-fit parameter spaces for the 2HDM+S model as well as the MED scenario,  $2 \rightarrow 2$  processes, and an Einasto halo in the Milky-Way. The limits are presented as the upper and lower edges of contour for each mass. Top right: Fermi-LAT GeV gamma-rays. Top Left: AMS-02 positrons. Bottom: AMS-02 anti-protons.

For any MeerKAT  $5\sigma$  detection prospects across the mass range, at least 1000 hours of observation time would be necessary. Notably this when  $B_0 = 1 \mu\text{G}$  and  $m_\chi = 200 \text{ GeV}$ . Despite this, the two-fold sensitivity advantage over previous observations of Reticulum II suggest that even 20 hours on target would yield cutting edge model-independent constraints on channels like  $b$  quarks. For the 2HDM+S model, when  $B_0 = 1 \mu\text{G}$ , 20 hours would translate to a 95% confidence interval limit of  $\langle\sigma V\rangle \lesssim 7 \times 10^{-26} \text{ cm}^3 \text{ s}^{-1}$  and  $M_\chi = 75 \text{ GeV}$ . The limit for 200 GeV WIMPs is around an order of magnitude larger.

The fact that detection would require at least 1000 hours of MeerKAT observation time suggests that this is improbable when  $B_0 = 1 \mu\text{G}$ . However, an increase in sensitivity to  $0.5 \mu\text{Jy beam}^{-1}$  would drop the required time to at least 40 hours. Thus, obtaining sub-micro-Jansky sensitivities starts to bring about the practical possibility of detection. This, however, would require the full SKA [42]. It should be noted that sufficient sensitivity for  $2\sigma$  exclusion of 2HDM+S model at the relic level, with the lowest studied DM mass, can be obtained with at least 100 hours

$M_\chi$ (GeV)	Lower ( $10^{-26} \text{ cm}^3 \text{ s}^{-1}$ )	Upper ( $10^{-26} \text{ cm}^3 \text{ s}^{-1}$ )	$M_\chi$ (GeV)	Lower ( $10^{-26} \text{ cm}^3 \text{ s}^{-1}$ )	Upper ( $10^{-26} \text{ cm}^3 \text{ s}^{-1}$ )
75.0	4.1	5.2	115.2	12.1	12.7
81.1	4.6	5.9	128.2	12.4	15.4
87.1	5.2	6.7	141.2	13.3	17.9
93.2	6.1	7.7	154.2	14.4	21.3
99.2	7.4	9.0	167.2	16.3	25.2
105.3	7.7	9.6	180.2	18.9	29.9
111.3	7.9	10.2	193.2	23.8	33.5
117.4	8.2	10.7	206.3	29.9	34.3
123.5	8.4	11.2	219.3	31.6	36.7
129.5	8.8	11.8	232.3	33.5	40.2
135.6	9.2	12.3	245.3	35.9	43.2
141.6	9.6	12.8	258.3	38.5	47.0
147.7	10.2	13.2	271.3	42.2	50.7
153.8	11.0	13.5	284.4	46.9	54.4
159.8	12.5	13.1	297.4	54.4	57.0

$M_\chi$ (GeV)	Lower ( $10^{-26} \text{ cm}^3 \text{ s}^{-1}$ )	Upper ( $10^{-26} \text{ cm}^3 \text{ s}^{-1}$ )
75.0	2.2	14.5
87.4	2.7	17.5
99.8	3.3	21.6
112.2	3.6	24.0
124.7	4.0	26.9
137.1	4.4	30.2
149.5	5.0	33.9
161.9	5.7	38.1
174.3	6.7	42.1
186.7	8.3	44.2
199.1	11.1	41.0
211.5	12.6	39.4
224.0	14.5	37.6
236.4	17.1	34.4
248.8	24.4	26.1

**Table 2.** The  $3\sigma$  confidence interval best-fit parameter spaces for the 2HDM+S model as well as the MED scenario,  $2 \rightarrow 2$  processes, and an NFW halo in the Milky-Way. The limits are presented as the upper and lower edges of contour for each mass. Top right: Fermi-LAT GeV gamma-rays. Top Left: AMS-02 positrons. Bottom: AMS-02 anti-protons.

on MeerKAT or 6 hours on the sub-micro-Jansky case. The time required to probe a 200 GeV WIMP at the relic level is around one hundred times longer than the 75 GeV case. This is largely due to MeerKAT’s limited frequency coverage, which will be ameliorated in the full SKA.

One point to note is that of the sensitivity estimates, which are strictly applicable to point sources and a nearby dwarf galaxy like Reticulum II is likely to be extended on the order of arcminutes. To mitigate this somewhat we have only integrated the flux within 3 arcminutes of the centre of Reticulum II and assumed arcminute-scales when calculating the sensitivity. The search prospects will likely improve when a visibility taper is considered, as this suppresses the long array baselines, tuning the sensitivity towards larger scale emissions [40]. This consideration makes the presented results somewhat conservative.

In Fig. 5 we display the potential non-observation constraints from 100 hours of observation of Reticulum II with both MeerKAT and the SKA. MeerKAT can only probe the 2HDM+S model down to the thermal relic cross-section for DM masses  $\lesssim 75$  GeV. However, it can exclude

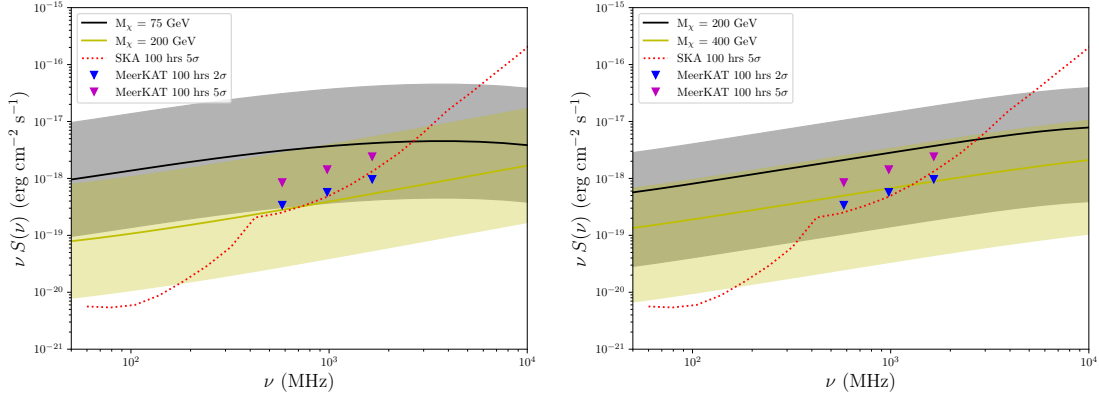


**Figure 4.** Radio spectrum prediction for Reticulum II with the Einasto profile. The shaded regions encompass the cross-section uncertainties from 2, as well as those from the J-factor of the halo and magnetic field. Left:  $2 \rightarrow 2$  scattering. Right:  $2 \rightarrow 3$  scattering.

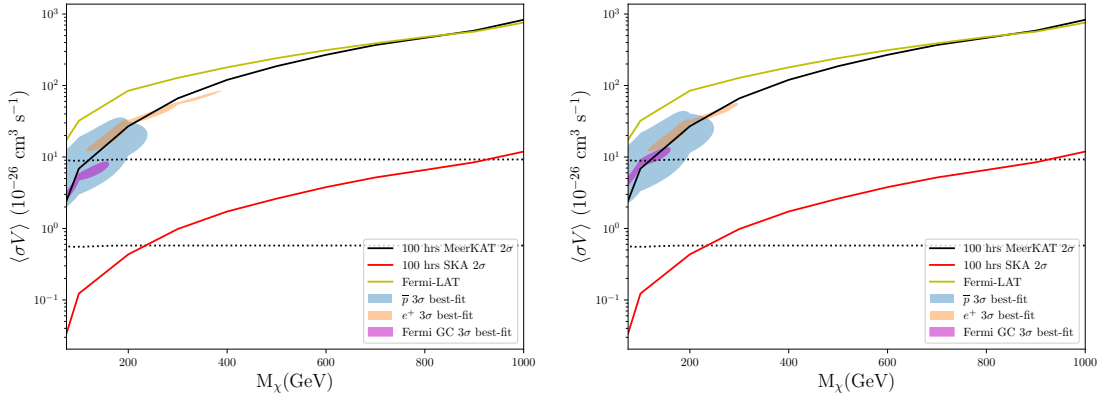


**Figure 5.** Non-observation  $2\sigma$  exclusion projections for Reticulum II (Einasto profile) with MeerKAT and the SKA. Left: Milkyway-Way galactic centre with Einasto profile. Right: Milkyway-Way galactic centre with NFW profile. The shaded regions are drawn from Fig. 2. The Fermi-LAT limits are drawn from data found in Ref. [64] and we use a  $30'$  integration region in this case.

a significant part of the excess overlap regions for the astrophysical excesses when  $\rho_\odot = 0.4 \text{ GeV cm}^{-3}$ , in both cases of NFW and Einasto density profiles for the Milky-Way. The current uncertainties in the local DM density mean the overlap region from Fig. 2 can potentially evade MeerKAT exclusion with 100 hours of observation time if the local density is  $\rho_\odot \sim 0.8 \text{ GeV cm}^{-3}$ . This is, however, an extreme scenario. Thus, MeerKAT shows considerable potential to probe the parameter space corresponding to the 2HDM+S DM candidate accounting for the studied astrophysical excesses. The potential upper limits are summarised in table 3. What is very notable is that the MeerKAT sensitivity estimates have highly competitive constraining power when compared to the Fermi-LAT data.

In figure 6 we display the limits on the coupling parameter between  $\chi$  and  $S$  that can be inferred from the results of figure 5 in the  $2 \rightarrow 2$  case. These demonstrate that this parameter space remains difficult to probe, however, for low  $M_\chi$  we see that the SKA has the potential to probe below  $g_\chi^S = 1$  (the  $2 \rightarrow 3$  case provides no real limits as the cross-section is much lower, suggesting it would be subdominant anyway). It is notable that this coupling is unconstrained by current LHC data.

$M_\chi$ (GeV)	MeerKAT ( $10^{-26} \text{ cm}^3 \text{ s}^{-1}$ )	SKA ( $10^{-26} \text{ cm}^3 \text{ s}^{-1}$ )
75	2.5	0.034
100	6.9	0.12
200	27	0.43
300	66	0.98
400	120	1.7
500	190	2.6
600	270	3.8
700	370	5.2
800	470	6.6
900	590	8.4
1000	830	12

**Table 3.** Potential non-observation upper limits on  $\langle\sigma V\rangle$  for the 2HDM+ $S$  model in the  $2 \rightarrow 2$  scenario. This data assumes the MED diffusion scenario and an Einasto halo profile in the Milky-Way.

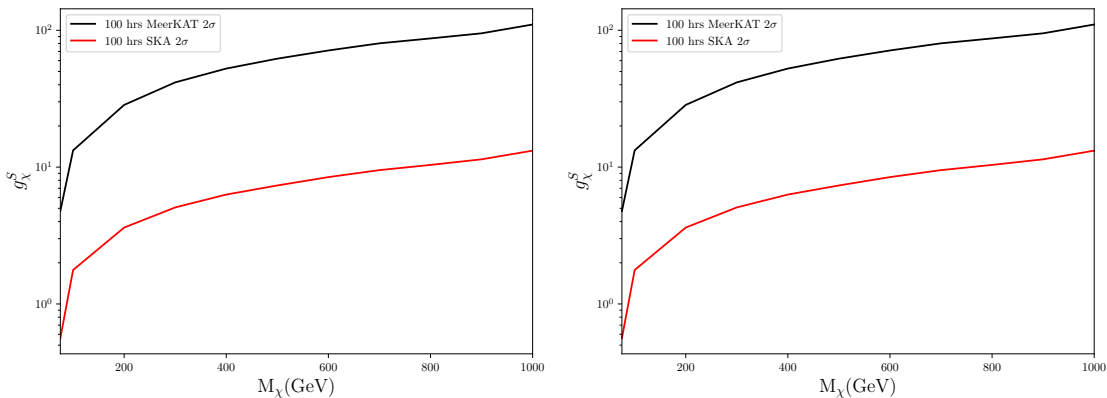


**Figure 6.** Non-observation  $2\sigma$  exclusion projections on the coupling between  $S$  and  $\chi$  ( $2 \rightarrow 2$  case) for Reticulum II (Einasto profile) with MeerKAT and the SKA. Left: Milky-Way galactic centre with Einasto profile. Right: Milky-Way galactic centre with NFW profile.

## 7 Conclusions

In this paper we used a 2HDM+ $S$  model, that describes the multi-lepton anomalies at the LHC, to describe the excesses in gamma-ray flux from the galactic centre and the cosmic-ray spectra from AMS-02. This is achieved through DM annihilation via the singlet scalar into particles of the SM. The parameters of the model are fixed to the LHC data, except for the mass of the DM and the size of the coupling to the mediator  $S$  (these being, as yet, unconstrained by collider data). The mass of the DM is scanned, where the coupling of the DM to the mediator  $S$  is varied, and various diffusion scenarios are considered. A satisfactory description of the gamma-ray flux from the galactic centre and the cosmic-ray spectra from AMS-02 is obtained with the MED diffusion scenario. The best description of the excesses is obtained for DM masses below 200GeV. Although complete overlap between all the best-fit regions is not achieved, it is notable that there are unresolved systematics in much of the data. Nonetheless, it is still remarkable that such close agreement can be obtained for a model whose particle physics is set by LHC anomalies.

Predictions of the synchrotron spectrum are made with the model in order to assess the detection sensitivity of MeerKAT in a conservative scenario where no visibility taper is considered. We conducted our test on a fiducial best-fit cross-section of  $10^{-25} \text{ cm}^3 \text{ s}^{-1}$  to characterise the region of overlap for the various excesses, and made use of only a 3 arcminute observation region and scaled point source sensitivity for MeerKAT. We found that  $5\sigma$  detection is possible, within 20

hours of observation at lower masses. However, around 1000 hours might be necessary to survey up to 200 GeV. This would still fail to cover the entire uncertainty region, so some of the parameter space can evade any conceivable detection with MeerKAT. This is not the case with the full SKA. Which, at  $5\sigma$  confidence interval and 100 hours observing time, can probe the entire uncertainty band for all masses in the excess overlap window. However, we note that an optimised MeerKAT search for diffuse emissions will likely have increased sensitivity.

It is worth highlighting that the MeerKAT sensitivity estimates have highly competitive constraining power, even somewhat exceeding that of Fermi-LAT data. MeerKAT can explore a significant area of the full excess overlap parameter space at  $2\sigma$  confidence level with 100 hours of observing time. Whereas, Fermi-LAT with data from [64] and a 10 times larger integration radius does not intrude at all upon these parameter regions. On the other hand, the full SKA can explore the entire overlap parameter space, even within uncertainties due to  $\rho_{\odot}$ , with less than 100 hours of observation. However, at present MeerKAT will be the frontier in radio instruments for DM searches, especially since it has begun observing calls already and will be upgraded in the near future with 30% more dishes.

The results documented in this work have implications on searches for DM at the LHC, due to the fact that limits on the cross-section from  $\chi\chi \rightarrow \text{SM}$  translate directly to the coupling between  $\chi$  and  $S$  in Eq. (3.2), as the other model parameters are fixed. Additionally, as an SM singlet,  $S$  is predominantly produced via the decay of the heavy scalar  $H \rightarrow SS$ . Thus, DM produced via the decay of  $S$  can recoil against SM particles that  $S$  can also decay into [9]. Of particular interest would be the resonant search for  $S \rightarrow ZZ, Z\gamma, \gamma\gamma$  in association with moderate missing transverse energy carried by the DM. The astrophysical data provides a consistency test as well as a narrowed region of focus, in which collider data can be used to further probe the properties of 2HDM+ $S$  with respect to its unconstrained degrees of freedom.

## Acknowledgments

The authors want to thank Andreas Crivellin and Bhupal Dev for most useful discussions. The authors are grateful for support from the South African Department of Science and Innovation through the SA-CERN program and the National Research Foundation for various forms of support. GB acknowledges the funding of the National Research Foundation through Thuthuka grant number 117969.

## References

- [1] P. W. Higgs, *Broken symmetries, massless particles and gauge fields*, *Phys. Lett.* **12** (1964) 132.
- [2] F. Englert and R. Brout, *Broken Symmetry and the Mass of Gauge Vector Mesons*, *Phys. Rev. Lett.* **13** (1964) 321.
- [3] P. W. Higgs, *Broken Symmetries and the Masses of Gauge Bosons*, *Phys. Rev. Lett.* **13** (1964) 508.
- [4] G. S. Guralnik, C. R. Hagen and T. W. B. Kibble, *Global Conservation Laws and Massless Particles*, *Phys. Rev. Lett.* **13** (1964) 585.
- [5] ATLAS collaboration, *Observation of a new particle in the search for the Standard Model Higgs boson with the ATLAS detector at the LHC*, *Phys. Lett. B* **716** (2012) 1 [1207.7214].
- [6] CMS collaboration, *Observation of a New Boson at a Mass of 125 GeV with the CMS Experiment at the LHC*, *Phys. Lett. B* **716** (2012) 30 [1207.7235].
- [7] CMS collaboration, *Study of the Mass and Spin-Parity of the Higgs Boson Candidate Via Its Decays to Z Boson Pairs*, *Phys. Rev. Lett.* **110** (2013) 081803 [1212.6639].
- [8] ATLAS collaboration, *Evidence for the spin-0 nature of the Higgs boson using ATLAS data*, *Phys. Lett. B* **726** (2013) 120 [1307.1432].
- [9] S. von Buddenbrock, N. Chakrabarty, A. S. Cornell, D. Kar, M. Kumar, T. Mandal et al., *Phenomenological signatures of additional scalar bosons at the LHC*, *Eur. Phys. J. C* **76** (2016) 580 [1606.01674].



- [10] S. von Buddenbrock, A. S. Cornell, A. Fadol, M. Kumar, B. Mellado and X. Ruan, *Multi-lepton signatures of additional scalar bosons beyond the Standard Model at the LHC*, *J. Phys. G* **45** (2018) 115003 [[1711.07874](#)].
- [11] S. Buddenbrock, A. S. Cornell, Y. Fang, A. Fadol Mohammed, M. Kumar, B. Mellado et al., *The emergence of multi-lepton anomalies at the LHC and their compatibility with new physics at the EW scale*, *JHEP* **10** (2019) 157 [[1901.05300](#)].
- [12] S. von Buddenbrock, R. Ruiz and B. Mellado, *Anatomy of inclusive  $t\bar{t}W$  production at hadron colliders*, *Phys. Lett. B* **811** (2020) 135964 [[2009.00032](#)].
- [13] Y. Hernandez, M. Kumar, A. S. Cornell, S.-E. Dahbi, Y. Fang, B. Lieberman et al., *The anomalous production of multi-lepton and its impact on the measurement of  $Wh$  production at the LHC*, *Eur. Phys. J. C* **81** (2021) 365 [[1912.00699](#)].
- [14] S. Buddenbrock, A. S. Cornell, Y. Fang, A. Fadol Mohammed, M. Kumar, B. Mellado et al., *The emergence of multi-lepton anomalies at the LHC and their compatibility with new physics at the EW scale*, *JHEP* **10** (2019) 157 [[1901.05300](#)].
- [15] A. Crivellin, Y. Fang, O. Fischer, A. Kumar, M. Kumar, E. Malwa et al., *Accumulating Evidence for the Associate Production of a Neutral Scalar with Mass around 151 GeV*, [2109.02650](#).
- [16] O. Fischer et al., *Unveiling Hidden Physics at the LHC*, in *Unveiling hidden Physics Beyond the Standard Model at the LHC*, 9, 2021, [2109.06065](#).
- [17] D. Sabatta, A. S. Cornell, A. Goyal, M. Kumar, B. Mellado and X. Ruan, *Connecting muon anomalous magnetic moment and multi-lepton anomalies at LHC*, *Chin. Phys. C* **44** (2020) 063103 [[1909.03969](#)].
- [18] N. Aghanim, Y. Akrami, M. Ashdown, J. Aumont, C. Baccigalupi, M. Ballardini et al., *Planck 2018 results*, *Astronomy & Astrophysics* **641** (2020) A6.
- [19] L. V. E. Koopmans and T. Treu, *The structure and dynamics of luminous and dark matter in the early-type lens galaxy of 0047-281 at  $z=0.485$* , *The Astrophysical Journal* **583** (2003) 606–615.
- [20] R. B. Metcalf, L. A. Moustakas, A. J. Bunker and I. R. Parry, *Spectroscopic gravitational lensing and limits on the dark matter substructure in q2237+0305*, *The Astrophysical Journal* **607** (2004) 43–59.
- [21] H. Hoekstra, H. Yee and M. D. Gladders, *Current status of weak gravitational lensing*, *New Astronomy Reviews* **46** (2002) 767–781.
- [22] L. A. Moustakas and R. B. Metcalf, *Detecting dark matter substructure spectroscopically in strong gravitational lenses*, *Monthly Notices of the Royal Astronomical Society* **339** (2003) 607–615.
- [23] S. von Buddenbrock, A. S. Cornell, E. D. R. Iarilala, M. Kumar, B. Mellado, X. Ruan et al., *Constraints on a 2HDM with a singlet scalar and implications in the search for heavy bosons at the LHC*, *J. Phys. G* **46** (2019) 115001 [[1809.06344](#)].
- [24] AMS COLLABORATION collaboration, *Towards understanding the origin of cosmic-ray positrons*, *Phys. Rev. Lett.* **122** (2019) 041102.
- [25] AMS COLLABORATION collaboration, *Antiproton Flux, Antiproton-to-Proton Flux Ratio, and Properties of Elementary Particle Fluxes in Primary Cosmic Rays Measured with the Alpha Magnetic Spectrometer on the International Space Station*, *Phys. Rev. Lett.* **117** (2016) 091103.
- [26] M. Ackermann, M. Ajello, A. Albert, W. B. Atwood, L. Baldini, J. Ballet et al., *The fermi galactic center  $geV$  excess and implications for dark matter*, *The Astrophysical Journal* **840** (2017) 43.
- [27] I. Cholis, T. Linden and D. Hooper, *A robust excess in the cosmic-ray antiproton spectrum: Implications for annihilating dark matter*, *Physical Review D* **99** (2019) .
- [28] A. Das, B. Dasgupta and A. Ray, *Galactic positron excess from selectively enhanced dark matter annihilation*, *Phys. Rev. D* **101** (2020) 063014.
- [29] K. Ishiwata, O. Macias, S. Ando and M. Arimoto, *Probing heavy dark matter decays with multi-messenger astrophysical data*, *Journal of Cosmology and Astroparticle Physics* **2020** (2020) 003.



- [30] Y. Farzan and M. Rajaei, *Dark matter decaying into millicharged particles as a solution to AMS-02 positron excess*, *Journal of Cosmology and Astroparticle Physics* **2019** (2019) 040.
- [31] S. Profumo, F. Queiroz and C. Siqueira, *Has AMS-02 Observed Two-Component Dark Matter?*, *J. Phys. G* **48** (2020) 015006 [1903.07638].
- [32] T. Li, *Revisiting simplified dark matter models in terms of ams-02 and fermi-lat*, *Journal of High Energy Physics* **2018** (2018) .
- [33] G. Giesen, M. Boudaud, Y. Génolini, V. Poulin, M. Cirelli, P. Salati et al., *Ams-02 antiprotons, at last! secondary astrophysical component and immediate implications for dark matter*, *Journal of Cosmology and Astroparticle Physics* **2015** (2015) 023–023.
- [34] G. Beck, *An excess of excesses examined via dark matter radio emissions from galaxies*, *Journal of Cosmology and Astroparticle Physics* **2019** (2019) 019–019.
- [35] G. Beck and S. Colafrancesco, *A Multi-frequency analysis of dark matter annihilation interpretations of recent anti-particle and  $\gamma$ -ray excesses in cosmic structures*, *JCAP* **1605** (2016) 013 [1508.01386].
- [36] W. Atwood, A. A. Abdo, M. Ackermann, W. Althouse, B. Anderson, M. Axelsson et al., *The large area telescope on the fermi gamma-ray space telescope mission*, *The Astrophysical Journal* **697** (2009) 1071.
- [37] P. Dewdney, W. Turner, R. Millenaar, R. McCool, J. Lazio and T. Cornwell, *Ska baseline design document*, .
- [38] S. Colafrancesco, P. Marchegiani and G. Beck, *Evolution of dark matter halos and their radio emissions*, *JCAP* **02** (2015) 032C.
- [39] M. Regis, L. Richter and S. Colafrancesco, *Dark matter in the reticulum ii dsph: a radio search*, *Journal of Cosmology and Astroparticle Physics* **2017** (2017) 025.
- [40] J. Marr, R. Snell and S. Kurtz, *Fundamentals of Radio Astronomy: Observational Methods*. CRC Press, 2015.
- [41] R. S. Booth, W. J. G. de Blok, J. L. Jonas and B. Fanaroff, *Meerkat key project science, specifications, and proposals*, 2009.
- [42] R. Braun, A. Bonaldi, T. Bourke, E. Keane and J. Wagg, *Anticipated performance of the square kilometre array – phase 1 (ska1)*, 2019.
- [43] M. Cirelli et al., *Pppc 4 dm id: A poor particle physicist cookbook for dark matter indirect detection*, *JCAP* **1103** (2011) 051.
- [44] D. Maurin, F. Donato, R. Taillet and P. Salati, *Cosmic rays below  $z=30$  in a diffusion model: new constraints on propagation parameters*, *The Astrophysical Journal* **555** (2001) 585.
- [45] E. A. Baltz and L. Wai, *Diffuse inverse compton and synchrotron emission from dark matter annihilations in galactic satellites*, *Physical Review D* **70** (2004) 023512.
- [46] E. A. Baltz and J. Edsjö, *Positron propagation and fluxes from neutralino annihilation in the halo*, *Physical Review D* **59** (1998) 023511.
- [47] S. Colafrancesco, S. Profumo and P. Ullio, *Multi-frequency analysis of neutralino dark matter annihilations in the coma cluster*, *Astronomy and Astrophysics* **455** (2006) 21.
- [48] S. Colafrancesco, S. Profumo and P. Ullio, *Detecting dark matter wimps in the draco dwarf: a multi-wavelength perspective*, *Physical Review D* **75** (2007) 023513.
- [49] M. Regis, S. Colafrancesco, S. Profumo, W. de Blok, M. Massardi and L. Richter, *Local group dsph radio survey with atca (iii): constraints on particle dark matter*, *Journal of Cosmology and Astroparticle Physics* **2014** (2014) 016–016.
- [50] A. E. Egorov and E. Pierpaoli, *Constraints on dark matter annihilation by radio observations of M31*, *Physical Review D* **88** (2013) 023504 [1304.0517].
- [51] M. S. Longair, *High Energy Astrophysics*. Cambridge University Press, 1994.
- [52] G. B. Rybicki and A. P. Lightman, *Radiative Processes in Astrophysics*. Wiley, June, 1986.

- [53] J. Alwall, M. Herquet, F. Maltoni, O. Mattelaer and T. Stelzer, *MadGraph 5 : Going Beyond*, *JHEP* **06** (2011) 128 [[1106.0522](#)].
- [54] T. Sjöstrand, S. Mrenna and P. Skands, *A brief introduction to pythia 8.1*, *Computer Physics Communications* **178** (2008) 852–867.
- [55] J. Heisig, M. Korsmeier and M. W. Winkler, *Dark matter or correlated errors: Systematics of the ams-02 antiproton excess*, *Physical Review Research* **2** (2020) .
- [56] K. Fang, X.-J. Bi and P.-F. Yin, *Reanalysis of the pulsar scenario to explain the cosmic positron excess considering the recent developments*, *The Astrophysical Journal* **884** (2019) 124.
- [57] M. D. Mauro, F. Donato, N. Fornengo and A. Vittino, *Dark matter vs. astrophysics in the interpretation of ams-02 electron and positron data*, *Journal of Cosmology and Astroparticle Physics* **2016** (2016) 031–031.
- [58] M. Di Mauro, *Characteristics of the galactic center excess measured with 11 years of fermi -lat data*, *Physical Review D* **103** (2021) .
- [59] J. F. Navarro, C. S. Frenk and S. D. M. White, *The Structure of cold dark matter halos*, *The Astrophysical Journal* **462** (1996) 563 [[astro-ph/9508025](#)].
- [60] G. Steigman, B. Dasgupta and J. F. Beacom, *Precise Relic WIMP Abundance and its Impact on Searches for Dark Matter Annihilation*, *Phys. Rev.* **D86** (2012) 023506 [[1204.3622](#)].
- [61] M. Weber and W. de Boer, *Determination of the local dark matter density in our galaxy*, *Astronomy and Astrophysics* **509** (2010) A25.
- [62] M. Benito, A. Cuoco and F. Iocco, *Handling the uncertainties in the galactic dark matter distribution for particle dark matter searches*, *Journal of Cosmology and Astroparticle Physics* **2019** (2019) 033–033.
- [63] N. F. Bell, G. Busoni and I. W. Sanderson, *Self-consistent Dark Matter Simplified Models with an s-channel scalar mediator*, *JCAP* **03** (2017) 015 [[1612.03475](#)].
- [64] FERMI-LAT AND DES COLLABORATIONS collaboration, *Searching for dark matter annihilation in recently discovered milky way satellites with fermi-lat*, *The Astrophysical Journal* **834** (2017) 110.
- [65] M. G. Walker, M. Mateo, E. W. Olszewski, J. P. narubia, N. W. Evans and G. Gilmore, *A universal mass profile for dwarf spheroidal galaxies?*, *ApJ* **704** (2009) 1274.
- [66] J. J. Adams et al., *Dwarf galaxy dark matter density profiles inferred from stellar and gas kinematics*, *ApJ* **789** (2014) 63.
- [67] J. Einasto, *On galactic descriptive functions*, *Publications of the Tartuskoj Astrofizica Observatory* **36** (1968) 414.
- [68] DES COLLABORATION collaboration, *Eight New Milky Way Companions Discovered in First-year Dark Energy Survey Data*, *ApJ* **807** (2015) 50 [[1503.02584](#)].
- [69] S. E. Koposov, V. Belokurov, G. Torrealba and N. W. Evans, *Beasts of the Southern Wild: Discovery of nine Ultra Faint satellites in the vicinity of the Magellanic Clouds*, *ApJ* **805** (2015) 130 [[1503.02079](#)].